

AD-A226 268

2

TECHNICAL REPORT BRL-TR-3129

BRL

DTIC FILE COPY

BEHAVIOR OF SEGMENTED RODS DURING PENETRATION

**G.E. HAUVER
A. MELANI**

JULY 1990

**DTIC
ELECTE
SEP 10 1990
S B D**

APPROVED FOR PUBLIC RELEASE; DISTRIBUTION UNLIMITED.

U.S. ARMY LABORATORY COMMAND

**BALLISTIC RESEARCH LABORATORY
ABERDEEN PROVING GROUND, MARYLAND**

NOTICES

Destroy this report when it is no longer needed. DO NOT return it to the originator.

Additional copies of this report may be obtained from the National Technical Information Service, U.S. Department of Commerce, 5285 Port Royal Road, Springfield, VA 22161.

The findings of this report are not to be construed as an official Department of the Army position, unless so designated by other authorized documents.

The use of trade names or manufacturers' names in this report does not constitute indorsement of any commercial product.

UNCLASSIFIED

REPORT DOCUMENTATION PAGE			Form Approved OMB No. 0704-0188	
Public reporting burden for this collection of information is estimated to average 1 hour per response, including the time for reviewing instructions, searching existing data sources, gathering and maintaining the data needed, and completing and reviewing the collection of information. Send comments regarding this burden estimate or any other aspect of this collection of information, including suggestions for reducing this burden, to Washington Headquarters Services, Directorate for Information Operations and Reports, 1215 Jefferson Davis Highway, Suite 1204, Arlington, VA 22202-4302, and to the Office of Management and Budget, Paperwork Reduction Project (0704-0188), Washington, DC 20503				
1. AGENCY USE ONLY (Leave blank)		2. REPORT DATE July 1990		3. REPORT TYPE AND DATES COVERED Final May 86 - May 88
4. TITLE AND SUBTITLE Behavior of Segmented Rods During Penetration			5. FUNDING NUMBERS 1L161102AH43	
6. AUTHOR(S) G. E. Hauver, A. Melani				
7. PERFORMING ORGANIZATION NAME(S) AND ADDRESS(ES)			8. PERFORMING ORGANIZATION REPORT NUMBER	
9. SPONSORING / MONITORING AGENCY NAME(S) AND ADDRESS(ES) Ballistic Research Laboratory ATTN: SLCBR-DD-T Aberdeen Proving Ground, MD 21005-5066			10. SPONSORING / MONITORING AGENCY REPORT NUMBER BRL-TR-3129	
11. SUPPLEMENTARY NOTES				
12a. DISTRIBUTION / AVAILABILITY STATEMENT Approved for public release; distribution is unlimited.			12b. DISTRIBUTION CODE	
13. ABSTRACT (Maximum 200 words) → Flash radiographic observations and measurements were used to examine the behavior of small-scale segmented and unitary rods as they penetrated steel targets after impact at 1500 m/s. Penetration data were examined by an eroding-rod model which aided the interpretations of behavior. Segmented rods of tungsten alloy always penetrated less than the equivalent unitary rod. Successive rod segments were found to contribute progressively less to the total penetration because of their interactions with residue and erosion products. A few experiments were conducted with gold-alloy penetrators because unitary rods of this material surpassed the performance of unitary tungsten-alloy rods, while leaving almost no residue at the end of penetration. However, segmented rods of the gold alloy performed poorly because their low strength made them susceptible to severe damage during the encounter with erosion products. A thin tubular support of aluminum or steel was found to improve the performance of tungsten-alloy segments, and possible reasons for the improvement are discussed.				
14. SUBJECT TERMS Segmented Penetrator; Long Rod Penetrator; Penetration; Kinetic Energy Penetration; Terminal Ballistics; Reverse Ballistics			15. NUMBER OF PAGES 38	
			16. PRICE CODE	
17. SECURITY CLASSIFICATION OF REPORT UNCLASSIFIED		18. SECURITY CLASSIFICATION OF THIS PAGE UNCLASSIFIED		19. SECURITY CLASSIFICATION OF ABSTRACT UNCLASSIFIED
				20. LIMITATION OF ABSTRACT SAR

NSN 7540-01-280-5500

UNCLASSIFIEDStandard Form 298 (Rev 2-89)
Prescribed by ANSI Std Z39-18
298-102

INTENTIONALLY LEFT BLANK.

TABLE OF CONTENTS

	LIST OF FIGURES	v
1.	INTRODUCTION	1
2.	EXPERIMENTAL PROCEDURE	1
3.	EXPERIMENTS, RESULTS, AND DISCUSSION	5
3.1	Experiment (WA, 1, 20)	5
3.2	Experiment (WA, 1, 4)	8
3.3	Experiment (WA, 2, 4, .5)	8
3.4	Experiment (WA, 2, 4, 2)	11
3.5	Experiment (WA, 5, 4, .5)	15
3.6	Experiment (WA, 2, 4, 1)	19
3.7	Experiment (AU, 1, 20)	19
3.8	Experiment (AU, 1, 4)	21
3.9	Experiment (AU, 5, 4, 1)	25
3.10	Experiments (WA/AL, 5, 4, 1) and (WA/SS, 5, 4, 1)	25
4.	CONCLUSION AND DISCUSSION	28
5.	REFERENCES	29
	DISTRIBUTION LIST	31



Accession For	
NTIS GRA&I	<input checked="" type="checkbox"/>
DTIC TAB	<input type="checkbox"/>
Unannounced	<input type="checkbox"/>
Justification	
By	
Distribution/	
Availability Codes	
Dist	Avail and/or Special
A-1	

INTENTIONALLY LEFT BLANK.

LIST OF FIGURES

<u>Figure</u>	<u>Page</u>
1 Target Area of the Light-Gas Gun	2
2 Close-Up View of the Target Area	3
3 Segments Supported by Foam	4
4 Schematic List of Experiments	6
5 Radiographs Showing Penetration by a Unitary Tungsten-Alloy Rod	7
6 Penetration-Time Plot for a Unitary Tungsten- Alloy Rod Penetrating Steel	9
7 Penetration-Time Plot for a Single Tungsten- Alloy Segment Penetrating Steel	10
8 Penetration-Time Plot for Two Tungsten-Alloy Segments Penetrating Steel	12
9 Radiographs Showing Penetration by Two Tungsten- Alloy Segments	13
10 Penetration-Time Plot for Two Tungsten-Alloy Segments Penetrating Steel	14
11 Target Sections	16
12 Radiographs Showing Penetration by Five Tungsten- Alloy Segments	17
13 Penetration-Time Plot for Five Tungsten-Alloy Segments Penetrating Steel	18
14 Radiographs Showing Penetration by a Unitary Gold-Alloy Rod	20
15 Penetration-Time Plot for a Unitary Gold-Alloy Rod Penetrating Steel	22
16 Radiographs Showing Penetration by a Single Gold-Alloy Segment	23
17 Penetration-Time Plot for a Single Gold-Alloy Segment Penetrating Steel	24

18	Radiographs Showing Penetration by Five Gold-Alloy Segments	26
19	Penetration-Time Plot for Five Gold-Alloy Segments Penetrating Steel	27

1. INTRODUCTION

Segmented rods, in principle, provide an advantage over unitary rods because they offer a multiple benefit from the transient high-pressure phase of penetration, while the delay between multiple impacts allows time for the penetration cavity to enlarge as a result of after flow (Pack and Evans 1951; Christman and Gehring 1966; Tate 1986). Although the performance of segmented penetrators should be enhanced at high impact velocities, small-scale experiments at the relatively low velocity of 1,500 m/s offered an opportunity to use reverse ballistics and megavolt flash radiography to examine the details of behavior within steel targets during penetration. Reverse ballistics overcame the problem of launching segmented rods and permitted experiments with either free-standing segments or supported segments. These experiments compared unitary and segmented rods, examined interactions between rod segments, considered the effect of segment strength, and examined the influence of a tubular support around the segments.

2. EXPERIMENTAL PROCEDURE

The small-scale, reverse-ballistic experiments were conducted in a single-stage light-gas gun. The target area of this gun, with an experiment in place, is shown in Figure 1. Two flash x-ray pulsers, supported above the target chamber, provided orthogonal views during penetration. Figure 2 shows a close-up view of the target area. A unitary rod is shown supported by fine threads in front of the muzzle. This rod is 1.58 mm in diameter and has a length-to-diameter (L/D) ratio of 20. Wire pairs were positioned before and behind the supported rod to provide electrical signals for measuring the impact velocity and triggering the x-ray pulsers. The targets were steel cylinders, 20 mm in diameter and up to 40 mm in length. These targets were launched in a polypropylene sabot, and each target carried a tungsten rod which served as a reference for penetration measurements. Although the method of support shown in Figure 2 was suitable for unitary rods, it was impractical in experiments with segmented rods. Figure 3 shows experiments in which polystyrene foam was used to support rod segments. The targets in these experiments had a hole drilled down the axis to simulate the penetration cavity. When segments were supported on the surface of a foam support, compression of the supporting foam was found to impart a rotation to each segment, as shown in the upper radiograph. However, with the segments enclosed in foam and with a "biscuit cutter" at the front of the target, the segments maintained their alignment within the simulated penetration cavity. This method of support was also useful with unitary rods and provided data identical to data obtained when unitary rods were supported by threads.

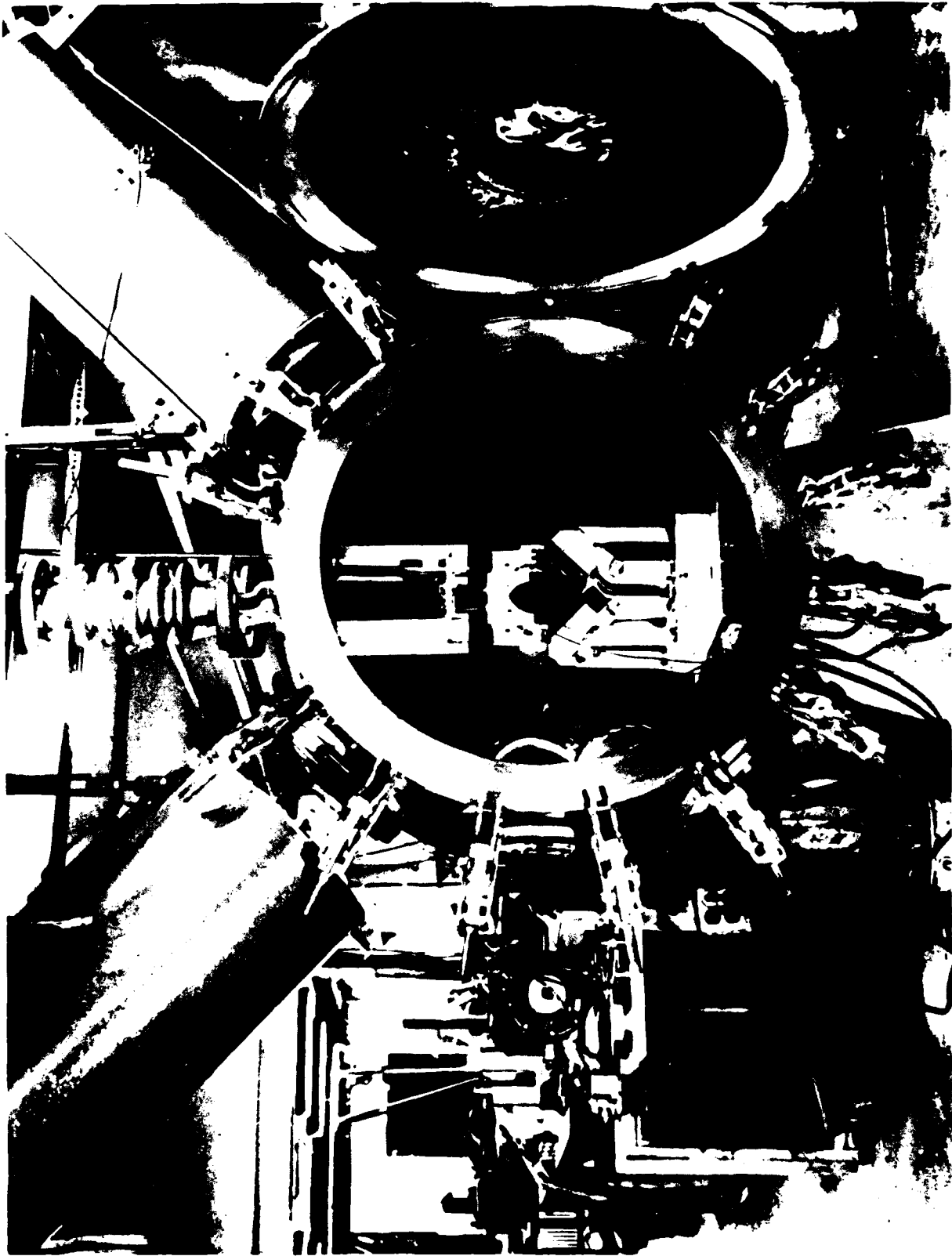


Figure 1. Target Area of the Light-Gas Gun.

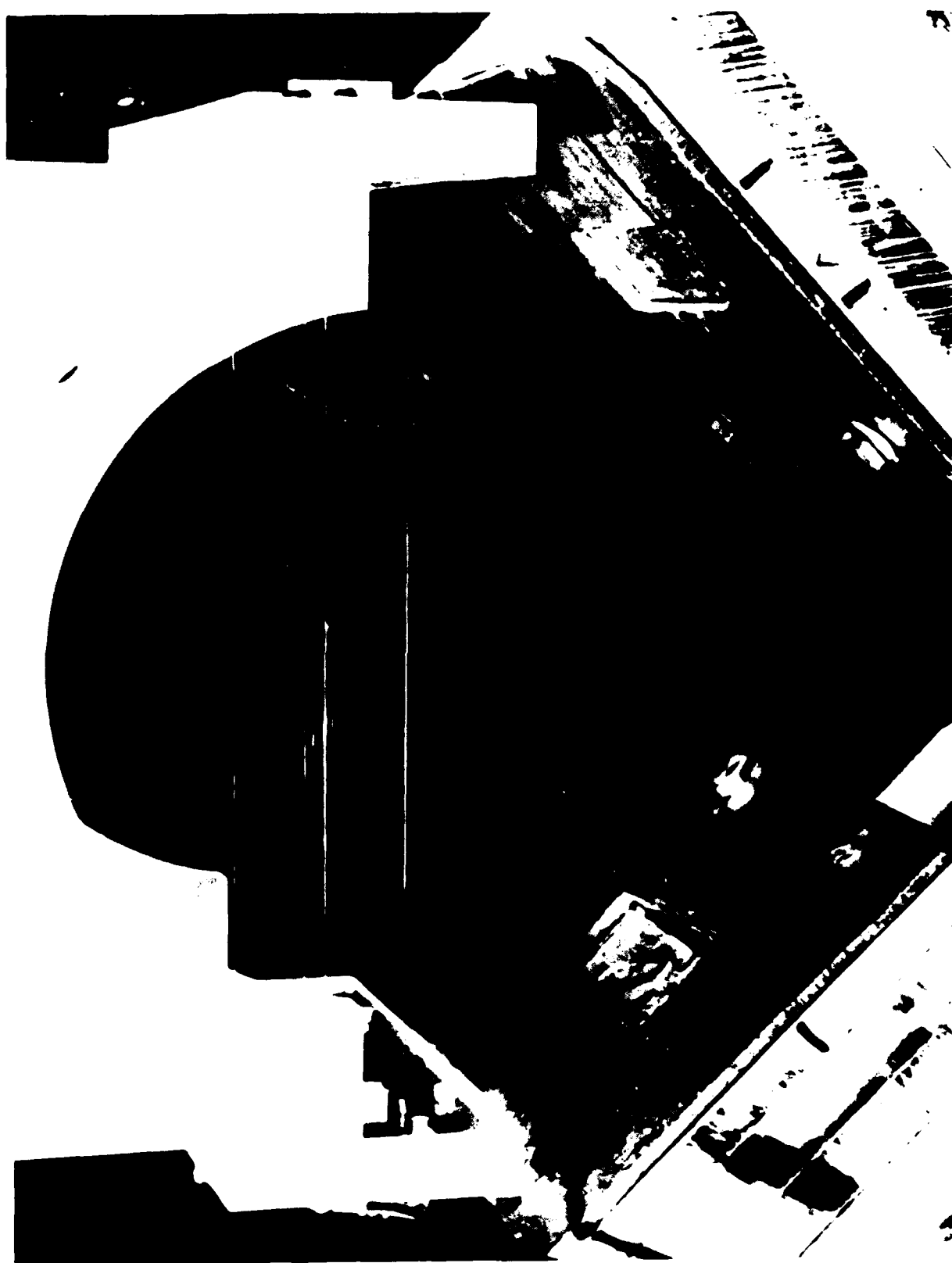


Figure 2. Close-Up View of the Target Area.

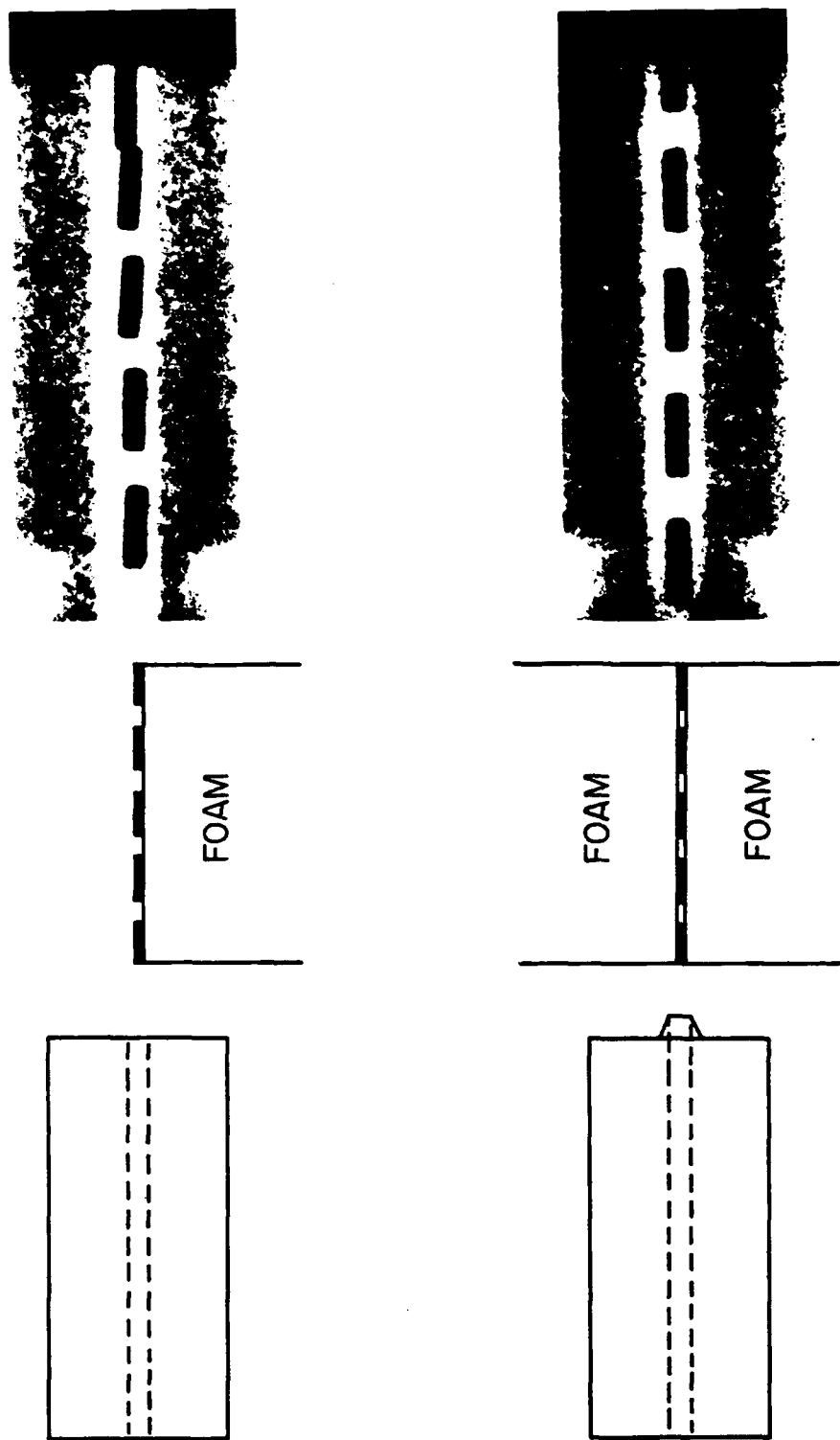


Figure 3. Segments Supported by Foam.

The rod segments in all experiments had a length-to-diameter ratio of four. Five segments were considered to be equivalent to a unitary rod with $L/D=20$. The tungsten-alloy penetrator material was composed of 90W-7Ni-3Fe, and the small-scale rods were machined from full-scale penetrators which had been swaged 24%. The density of this tungsten alloy was 17.2 Mg/m^3 . Gold-alloy penetrators were composed of 92Au-4.9Ag-3.1Cu, and had a density of 18.0 Mg/m^3 . The targets in all experiments were made of S7 steel. This steel had been made by vacuum induction melting with vacuum arc remelting (VIMVAR process), and all targets were heat treated to a hardness of Rockwell C 30.

3. EXPERIMENTS, RESULTS, AND DISCUSSION

The sequence of experiments is represented schematically in Figure 4. The "penetrator" column lists penetrator material, number of segments, L/D ratio, and segment spacing relative to segment length (in the case of multiple segments). The "penetration" column lists depth of penetration in millimeters. Experiments with free-standing segments will each be described, analyzed with the aid of an eroding-rod model (Aleksevsii, 1966; Tate 1967; Tate 1969; Wright 1983; Wright and Frank 1987) and discussed to clarify penetration behavior. Experiments with segments in a supporting tube did not permit a reliable analysis, but a qualitative discussion will be provided. All experiments will be identified by nomenclature in the "penetrator" column.

3.1 Experiment (WA, 1, 20) Several experiments were conducted to obtain data as a unitary tungsten-alloy rod, with $L/D=20$, penetrated a steel target. The flash radiographs from one of these experiments are shown in Figure 5. A few qualitative observations are possible before considering the analysis of penetration data. The first material eroded from the rod flows forward into the target. In the later (lower) radiograph, concentrations of eroded material are evident in the penetration cavity behind the penetrating rod. In the earlier radiograph, the erosion products appear to converge toward the axis of penetration. This could indicate that the target undergoes elastic recovery after the penetration front passes, imparting a small radial velocity to the erosion products. In the earlier radiograph, the forward portion of the rod tends to be obscured by erosion products, suggesting some congestion in the penetration cavity. In the later radiograph, the rod is almost completely obscured, suggesting greater congestion.












<u>PENETRATOR</u>	<u>TEST CONFIGURATION</u>	<u>PENETRATION</u>
(WA, 1, 20)		22.3
(WA, 5, 4, 5)		20.7
(WA, 5, 4, 1)		15.9
(WA, 1, 4)		6.2
(WA, 2, 4, 5)		6.2 + 3.7
(WA, 2, 4, 2)		6.2 + 2.4
(AU, 1, 20)		23.7
(AU, 1, 4)		5.7
(AU, 5, 4, 1)		14.0
(WA/AL, 5, 4, 1)		19.5
(WA/SS, 5, 4, 1)		20.9

Figure 4. Schematic List of Experiments.

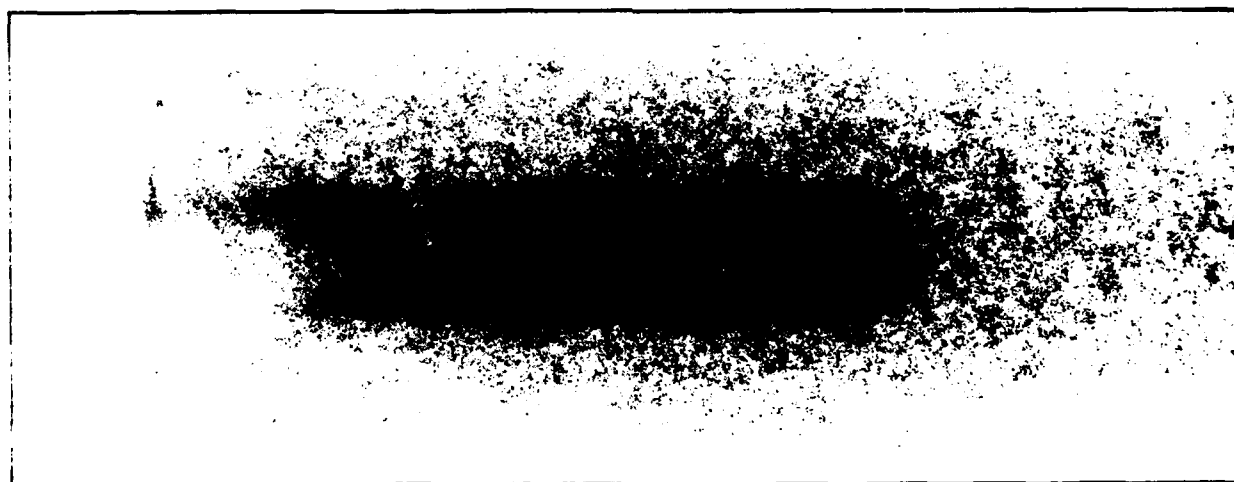


Figure 5. Radiographs Showing Penetration by a Unitary Tungsten-Alloy Rod.

Figure 6 is a penetration-time plot which presents the data and curves generated by the eroding-rod model. P_{MAX}, the maximum depth of penetration, is experimental data and was determined by direct measurement in sectioned targets. P_{MAX} in this experiment was 22.3 mm, as indicated in Figure 4. In applying the model, target resistance, R , was adjusted to produce agreement with the data. The low resistance just after impact is caused by the transient high-pressure phase of penetration. The gradual increase in resistance during penetration may relate to the increasing congestion evident in flash radiographs. Dashed paths with an arrow indicate the calculated motion of erosion products formed at selected times during the penetration. Intersection of the lower two dashed paths corresponds to the concentration of erosion products observed behind the penetrator in the lower radiograph in Figure 5. Congestion deeper in the penetration cavity may result from both the radial component of velocity and the opposing flows of erosion products from early and late times during the penetration. Later, these target resistances will be compared with values of target resistance from the analysis of penetration by a gold-alloy rod.

3.2 Experiment (WA, 1, 4). Chronologically, the experiments with five rod segments followed the experiments with unitary rods. When the data from these experiments could not be analyzed, experiments with one and two segments were conducted to provide additional information. The data from this experiment with a single segment are shown in Figure 7. P_{MAX} (6.2 mm) is a datum point obtained by measuring the recovered target. The low target resistance close to impact again results from the transient high-pressure phase of penetration. Agreement with the second datum point and P_{MAX} was achieved with $R=4.6$ GPa, a value much lower than values needed to describe deep penetration by the longer unitary rod. As in the case of a unitary rod, the convergent flow of erosion products is indicated by a pair of dashed lines. Residue is indicated at the end of penetration. The thickness of this residue was not calculated by the model but was measured from radiographs. This residue is not full-density tungsten alloy, and this complication will be discussed later.

3.3 Experiment (WA, 2, 4, 5). This experiment examined the penetration by two tungsten-alloy segments separated by half a segment length. Based on the test with a single segment, this spacing was judged to be near the minimum that should be used. With a smaller spacing, the second segment would overtake the first segment before its penetration was completed. It was anticipated that the minimum possible spacing would minimize any interaction between the erosion products and the second segment. This is important because this experiment was intended to evaluate the residue thickness and it was necessary to assume no interaction with erosion products.

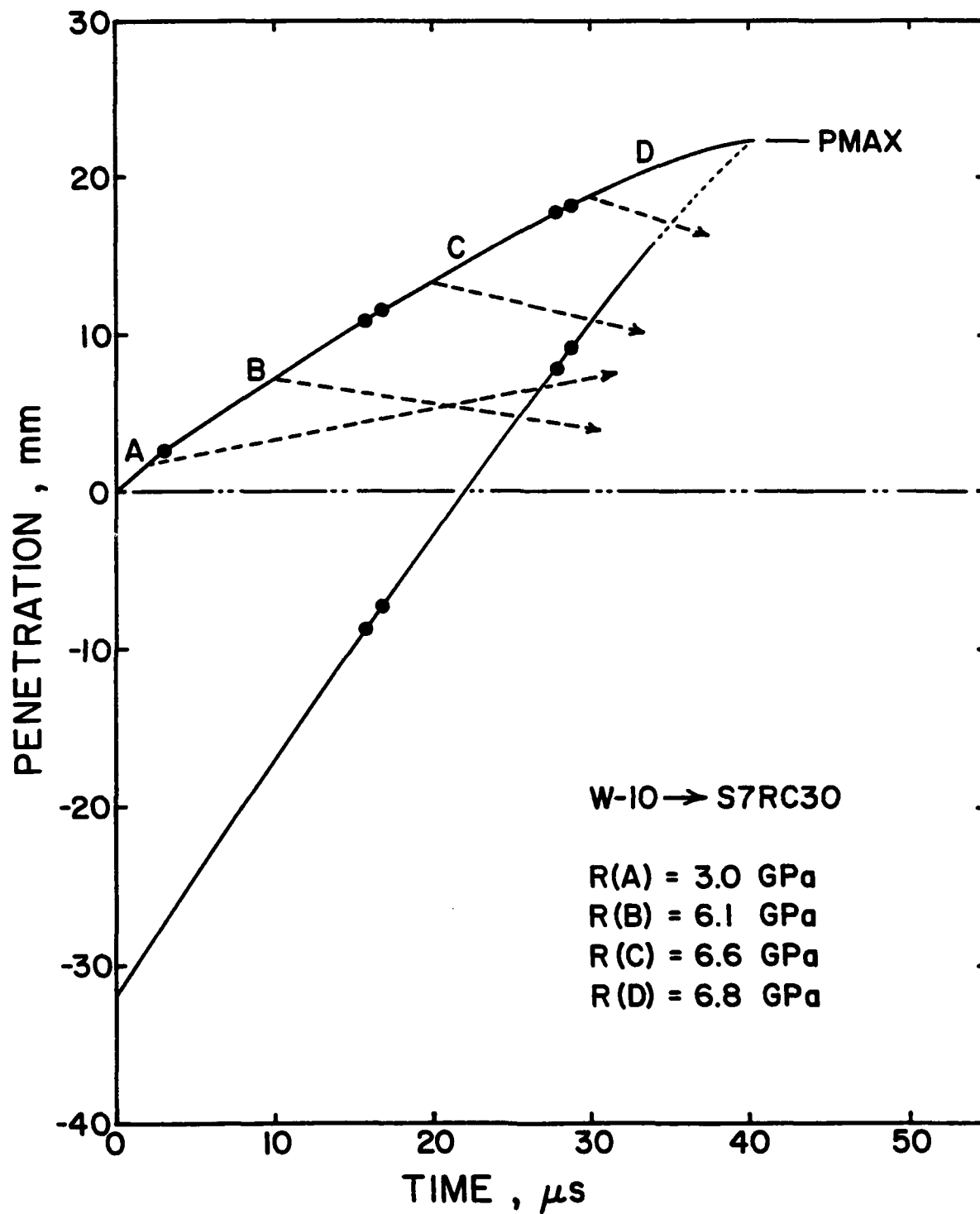


Figure 6. Penetration-Time Plot for a Unitary Tungsten-Alloy Rod Penetrating Steel.

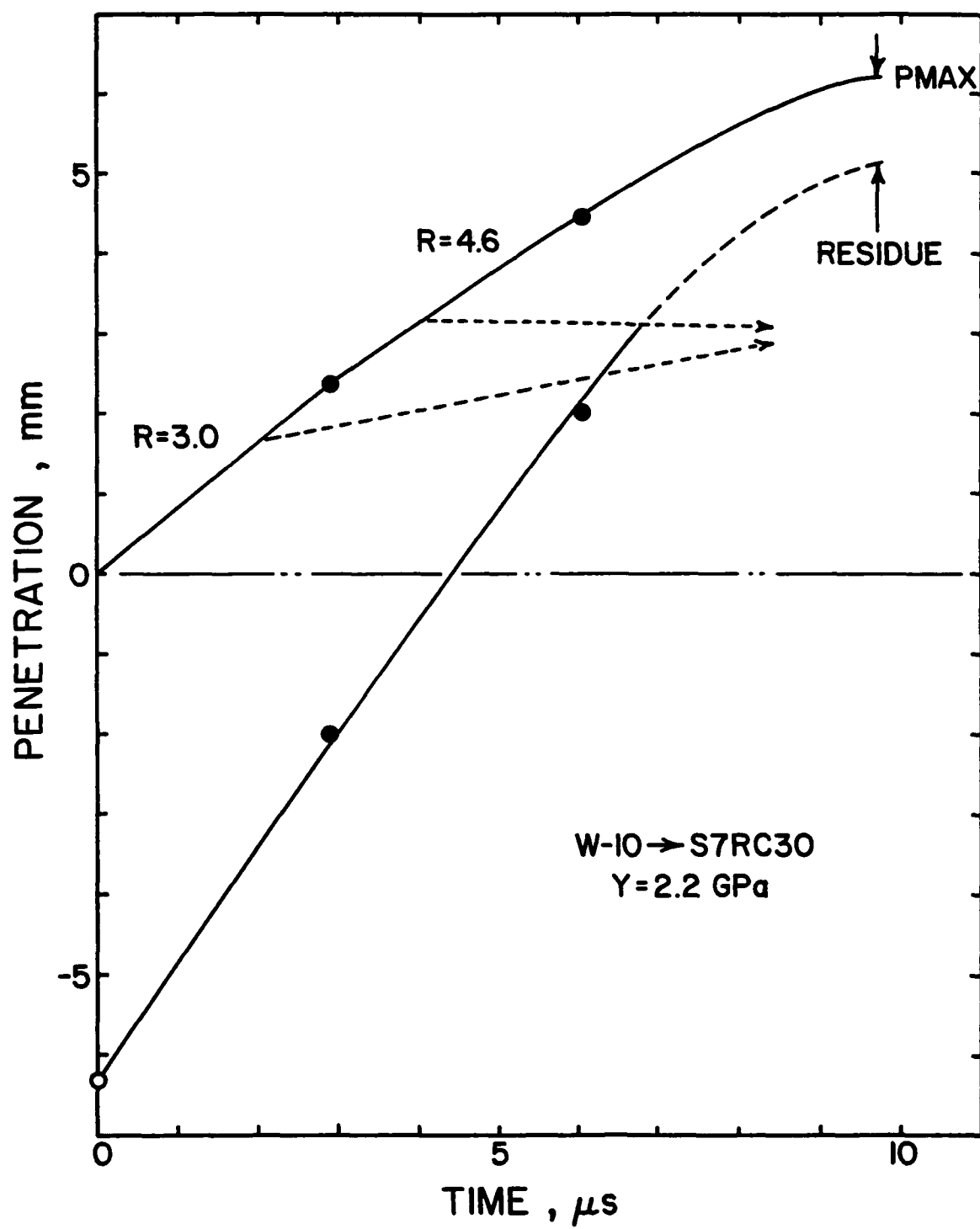


Figure 7. Penetration-Time Plot for a Single Tungsten-Alloy Segment Penetrating Steel.

The data from this experiment are shown in Figure 8 along with curves generated by the penetration model. Knowing the penetration by one segment, measuring the final penetration depth with two segments, and assuming no interaction with erosion products, it was necessary to assume a 1.37 mm thickness of full density tungsten-alloy residue. After penetrating this residue, the second segment was able to penetrate only an additional 3.7 mm of steel, making it just 60% as effective as the first segment.

3.4 Experiment (WA, 2, 4, 2). This experiment examined penetration by two segments under special conditions. The first segment impact occurred at the bottom of a recess which was drilled into the target to simulate the penetration cavity made by a single segment. This ensured that all erosion products would remain in the penetration cavity. By separating the segments by two segment lengths, observations could be made long after the completion of penetration by each segment, and there was a substantial time interval during which erosion products might migrate into the path of the second segment.

The flash radiographs from this experiment are shown in Figure 9. In the earlier (upper) radiograph, the second segment is shown just before impact against the deposit of residue left by the first segment. The front end of the second segment is deformed and its length has been reduced by 0.4 mm (6.5%) by the interaction with erosion products from the first segment. In the later radiograph (center), residue and erosion products remain in the penetration cavity after the second segment was fully consumed. If there were a third segment, it would encounter this debris from the first two segments. A static radiograph of the recovered target appears at the bottom. This radiograph shows the residue with improved resolution, but the lower-density erosion products are barely detected, although they are still present in the recovered target.

The data from this experiment are shown in Figure 10. Although the first segment again penetrated 6.2 mm, the second segment contributed only an additional 2.4 mm, making it just 39% as effective as the first segment. Again assuming a 1.37 mm thickness of full-density residue, it was further necessary to assume a 38 m/s reduction of velocity to account for the final depth of penetration. In Figure 10, there is a clear discrepancy between the calculated residue thickness of 1.37 mm and the thickness measured from flash radiographs. This was believed to result because the actual residue was less than full-density tungsten alloy.

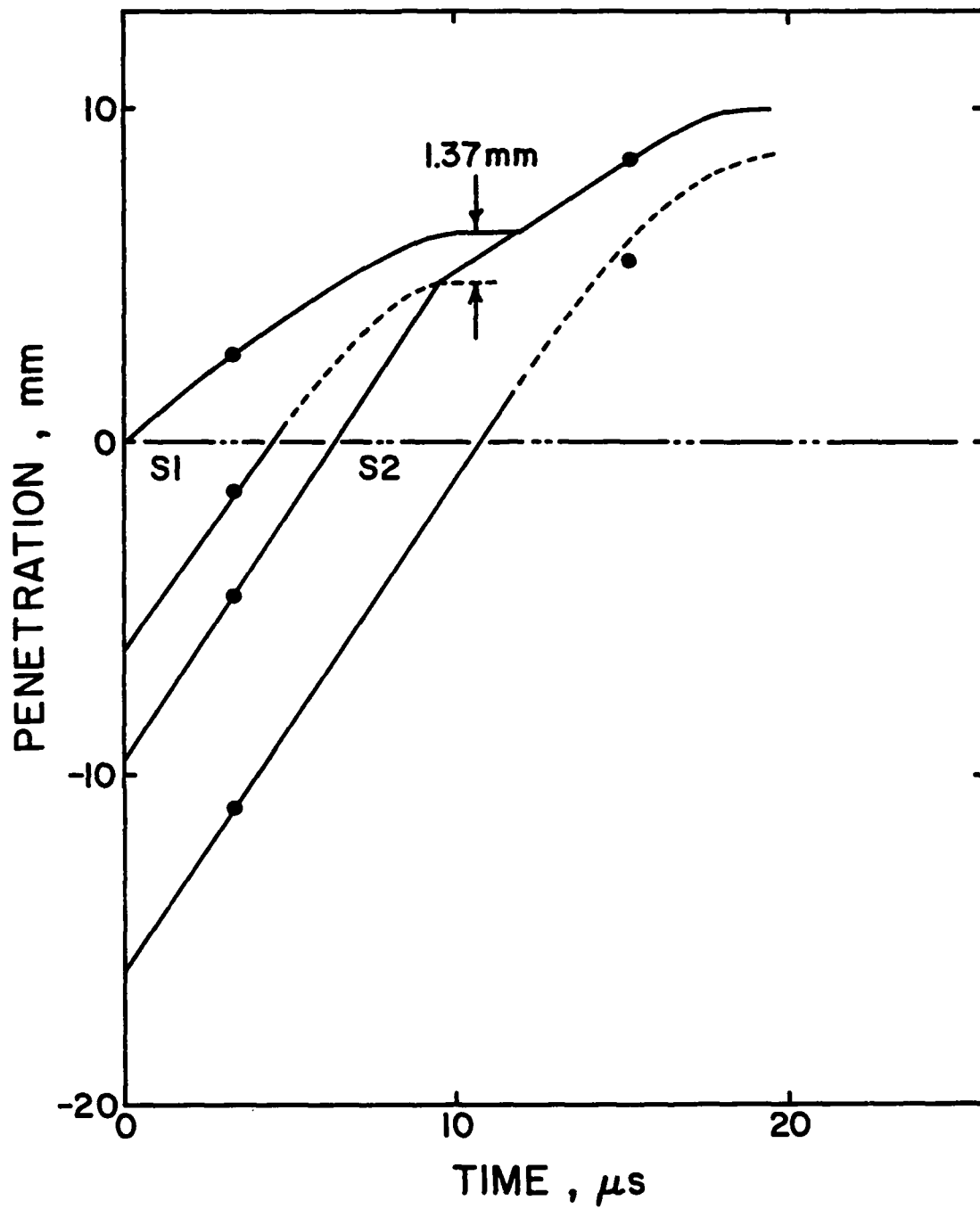


Figure 8. Penetration-Time Plot for Two Tungsten-Alloy Segments Penetrating Steel.

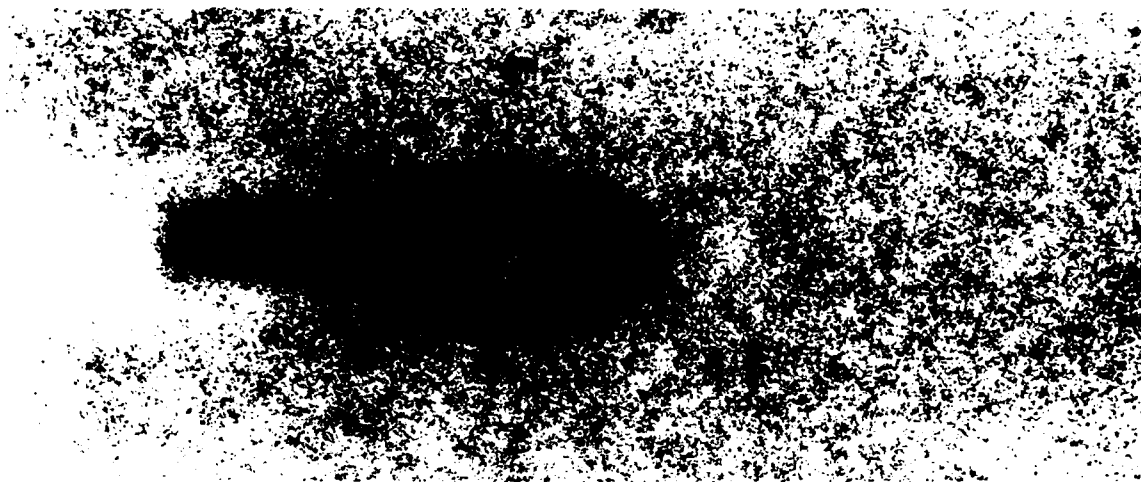


Figure 9. Radiographs Showing Penetration by Two Tungsten-Alloy Segments.

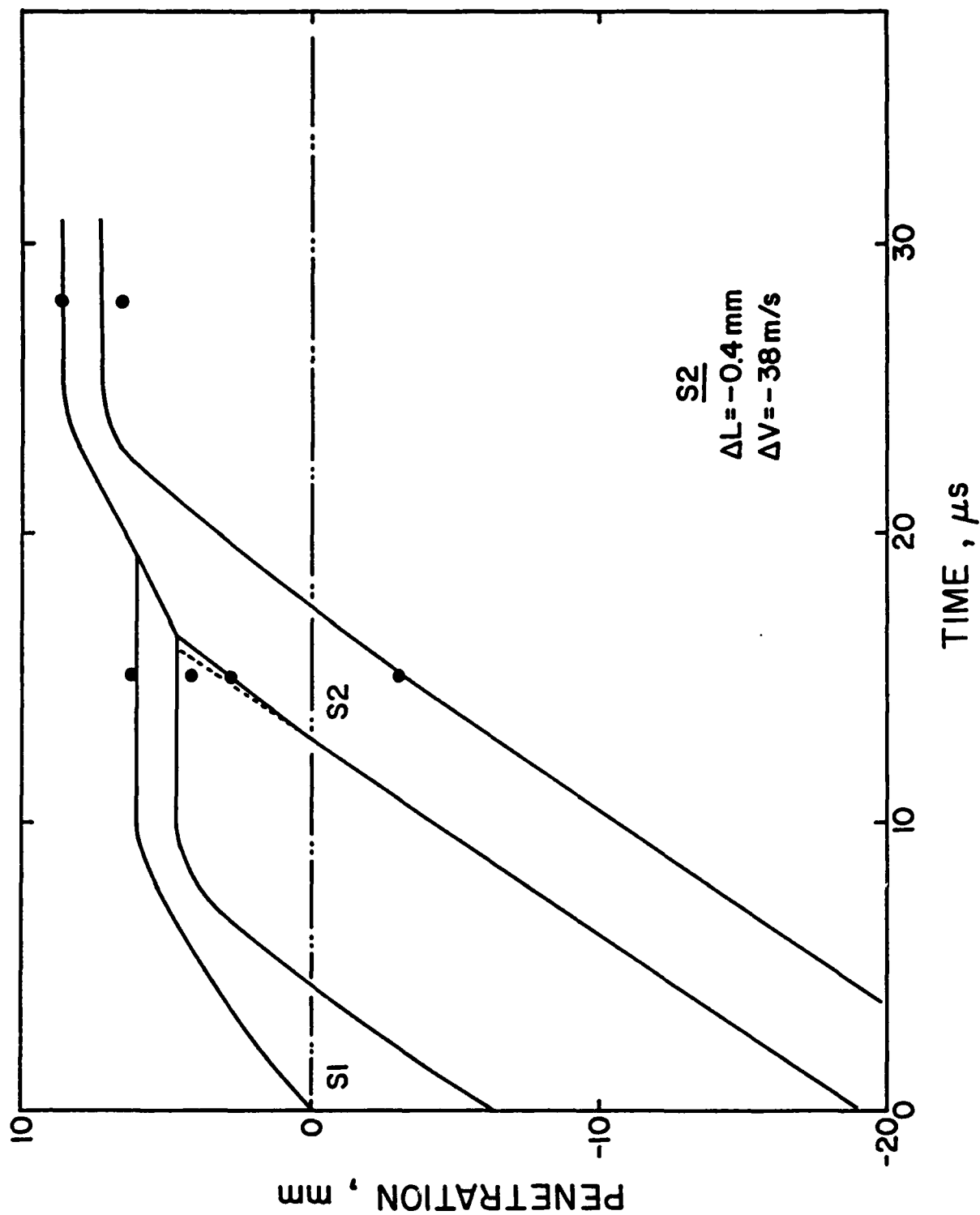


Figure 10. Penetration-Time Plot for Two Tungsten-Alloy Segments Penetrating Steel.

The target from this experiment was sectioned and examined. Photographs of the two sections are shown in Figure 11. The upper two photographs show the same section with different lighting. The small dark area near the end of penetration in the upper photograph is the only full-density penetrator material remaining (this is a light area in the center photograph). The surrounding material at the end of penetration is highly deformed tungsten alloy in various stages of failure. The erosion products were found to be a fragile, fine-grained metallic foam. They were inadvertently destroyed in the section at the top in Figure 11, but the foam remained in the other half of the target which is shown in the lower panel.

3.5 Experiment (WA, 5, 4, .5). The penetrator in this experiment consisted of five segments, separated by half a segment length. Figure 12 shows the radiographs taken during penetration, and a static radiograph of the recovered target. The first (upper) flash radiograph was taken during penetration by the third segment, and it also shows the trailing fourth and fifth segments. The second flash radiograph was taken during penetration by the fourth segment, and it also shows the trailing fifth segment. The two observations of the fifth segment allowed an evaluation of its average velocity within the penetration cavity. This average velocity was 1,374 m/s, well below the initial velocity of 1,493 m/s, but 90 m/s above the instantaneous impact velocity that later emerged from the analysis. The radiograph of the recovered target established the final penetration depth of 20.7 mm, 7.2% less than the depth of penetration by the equivalent unitary rod. The penetration cavity in the recovered target (lower panel) has a scalloped profile produced by the multiple-segment impacts. The radiographs strongly suggest that the cavity profile deflects moving erosion products and guides them toward the axis of penetration. The upper radiograph suggests that erosion products are impacting the side of the fourth segment. Also, the back end of each segment is much more clearly defined than the front end, suggesting an interaction with erosion products and some accumulation at the front of each segment. Possible erosion at the front of the fourth and fifth segments could not be reliably measured because of the accumulation.

The data and analysis for this experiment are shown in Figure 13. Penetration by the first two segments was based on the results from experiments with one and two segments. It is immediately apparent that conditions are different for the third, fourth, and fifth segments. The earliest erosion products from the first segment migrate forward into the penetration cavity. However, instead of encountering steel, the second segment first encounters residue of tungsten alloy and its earliest



Figure 11. Target Sections.



Figure 12. Radiographs Showing Penetration by Five Tungsten-Alloy Segments.

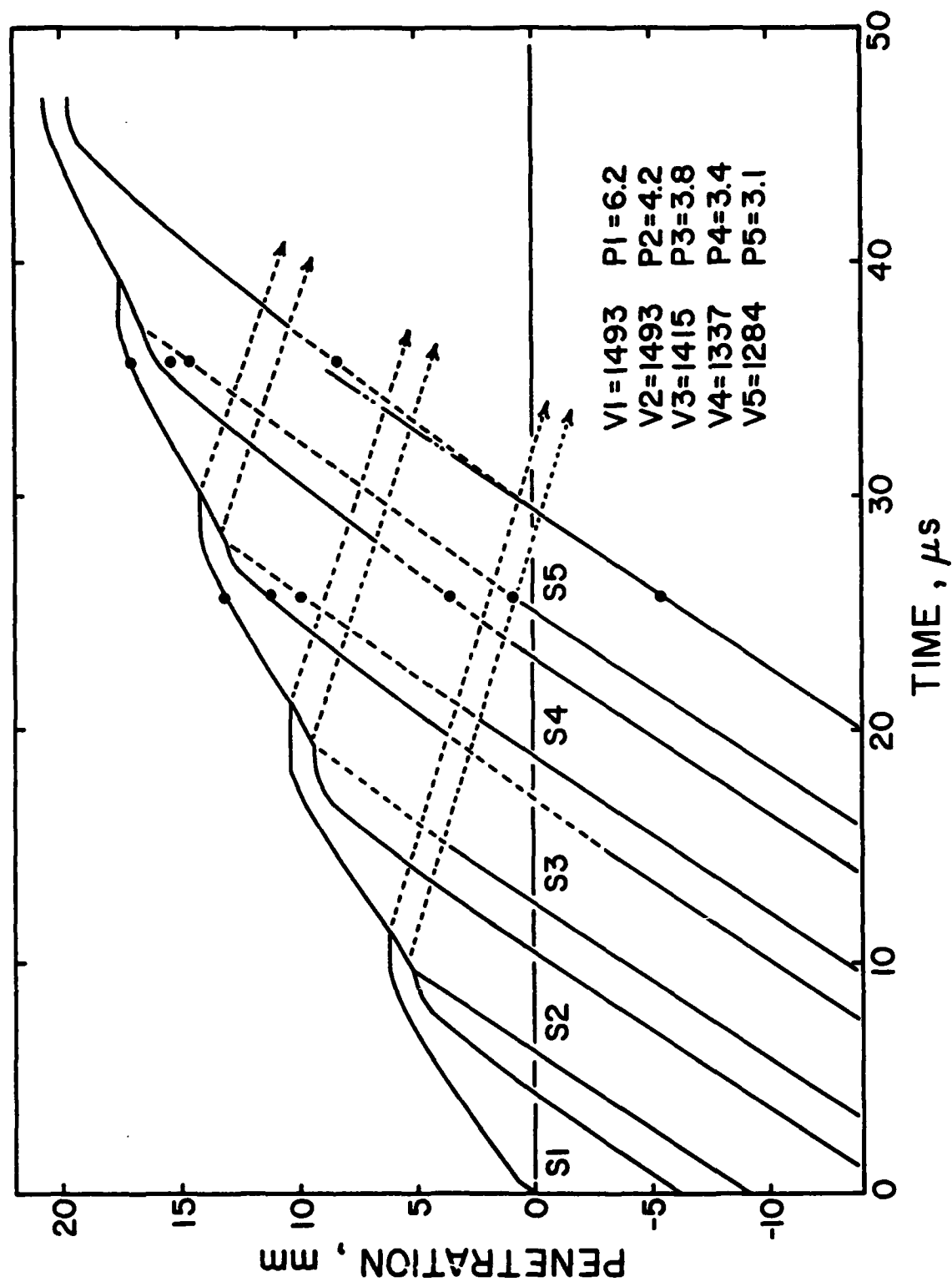


Figure 13. Penetration-Time Plot for Five Tungsten-Alloy Segments Penetrating Steel.

erosion products migrate backwards along the wall of the penetration cavity. A similar backward migration also occurs with the third and fourth segments. Consequently, the behavior suggested by radiographs is probably correct. The wall contour apparently deflects these earliest erosion products toward the axis of penetration, enhancing their interaction with trailing segments. Since the length of the third, fourth, and fifth segments could not be reliably measured prior to impact, it was necessary to attribute their decreased performance entirely to a decrease in velocity. In the case of the final segment, the calculated decrease in velocity was 209 m/s, or 14%. This decrease is undoubtedly somewhat too large because some loss of length must also have occurred. The progressive loss of performance is indicated in Figure 13, with the fifth segment contributing half the penetration of the first segment.

3.6 Experiment (WA, 2, 4, 1). The penetrator in this experiment also consisted of five free-standing segments, but the space between segments was increased to one segment length. The total penetration of only 15.9 mm indicated that the increased spacing permitted more serious degradation of the final three segments. By taking flash radiographs during penetration by the second and third segments, it was verified that the performance of the first two segments was the same as in the previous experiment (WA, 2, 4, .5). This caused some uncertainty about the exact contribution of the fourth and fifth segments, but the best estimate was a fifth-segment velocity of only 1071 m/s and a contribution of only 1.6 mm to the final depth of penetration.

3.7 Experiment (AU, 1, 20). The residue from tungsten alloy segments presented a twofold problem. It consumed part of the trailing segment and the erosion products formed during this penetration seemed to interact more destructively with trailing segments. Gold-alloy segments were considered as an alternative because the low strength of this material should minimize any residue. Initial experiments examined the penetration of a unitary rod, with $L/D=20$, into steel. Figure 14 shows flash radiographs recorded during penetration. Qualitatively, the observed penetration is significantly different from that observed with a unitary tungsten-alloy rod. The outline of the rod is clearly visible through the erosion products, including the mushroom tip at the end of the penetration cavity. No congestion in the penetration cavity is evident in the second radiograph where the outline of the rod is still clearly visible to the end of penetration. In this second radiograph, it is evident that some yaw has developed during the penetration. Also, there is no evidence that erosion products have acquired a radial component of velocity. This suggests that the convergence observed during penetration by a unitary tungsten-alloy rod may be characteristic of that material and not the target.

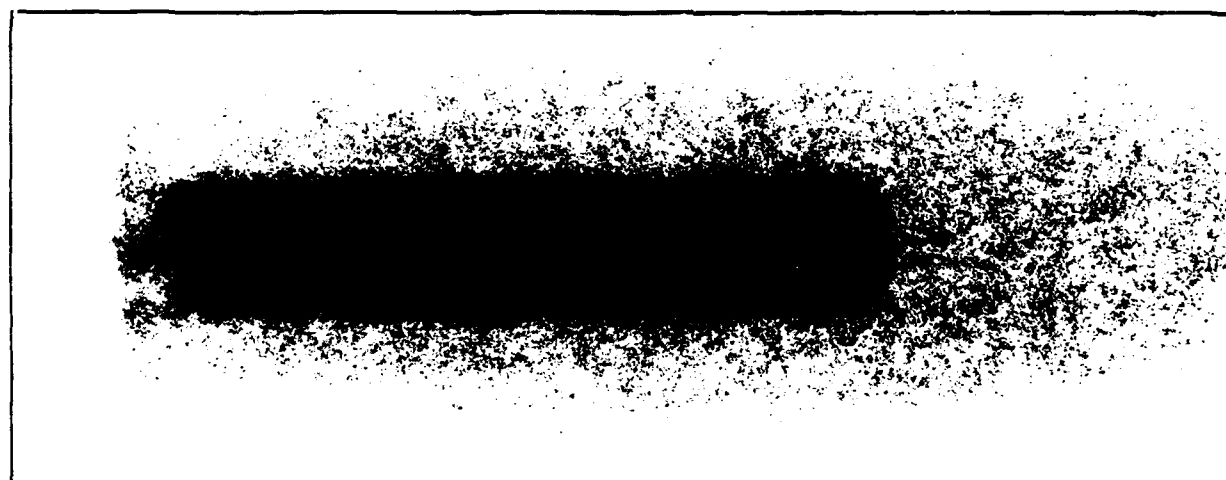


Figure 14. Radiographs Showing Penetration by a Unitary Gold-Alloy Rod.

The second radiograph indicates that the earliest erosion products have a small forward velocity relative to the target, and a concentration of the erosion products is observed just inside the target.

The data and analysis for this experiment are shown in Figure 15. The final depth of penetration, P_{MAX}, was 23.7 mm. This is 6.3% deeper than achieved with a tungsten-alloy rod with the same length, and it is slightly deeper penetration than would be anticipated on the basis of density alone. This final depth of penetration is also surprising because of the relatively low strength of the gold alloy. It is the low strength that causes a nearly linear path for the back end of the gold-alloy rod. The low resistance assigned close to impact results from the initial transient high-pressure phase of penetration. The resistance values required during deeper penetration are significantly lower than those required during penetration by a tungsten-alloy rod. Absence of congestion in the penetration cavity was apparent during penetration by the gold-alloy rod, and this may be related to the lower resistance values. Resistance to penetration clearly is not strictly a characteristic of the target material. This result is consistent with the derivation of the "Modified Bernoulli Equation" by Wright and Frank 1987, who concluded that the target resistance term is not simply dependent on target hardness but involves characteristics of the rod and of the specific collision under consideration. Again, dashed lines with an arrow indicate the flow of erosion products formed at selected times during the penetration. This indicated flow is consistent with qualitative observations about the radiographs. The earliest erosion products migrate forward at a low velocity relative to the target, and the concentration of erosion products observed in the lower radiograph of Figure 14 corresponds to an intersection of opposing flows.

3.8 Experiment (AU, 1, 4). One experiment with a single gold-alloy segment was conducted to aid the interpretation of the experiment with five segments. The radiographs during penetration by a single segment are shown in Figure 16. The second flash radiograph (center) shows that the segment is almost fully consumed 2 μ s (and approximately 1 mm) before the end of penetration. The static radiograph of the recovered target (lower panel) shows no evidence of residue at the end of penetration, which was the objective of introducing this material. Data and analysis for this experiment are shown in Figure 17. The final depth of penetration (P_{MAX}) is 5.7 mm. This is 8.1% less than the penetration produced by a single tungsten-alloy segment, which is more consistent with the performance anticipated on the basis of strength and density. Therefore, the superior performance of a long unitary rod of gold alloy must result from its superior interaction characteristics during deep penetration.

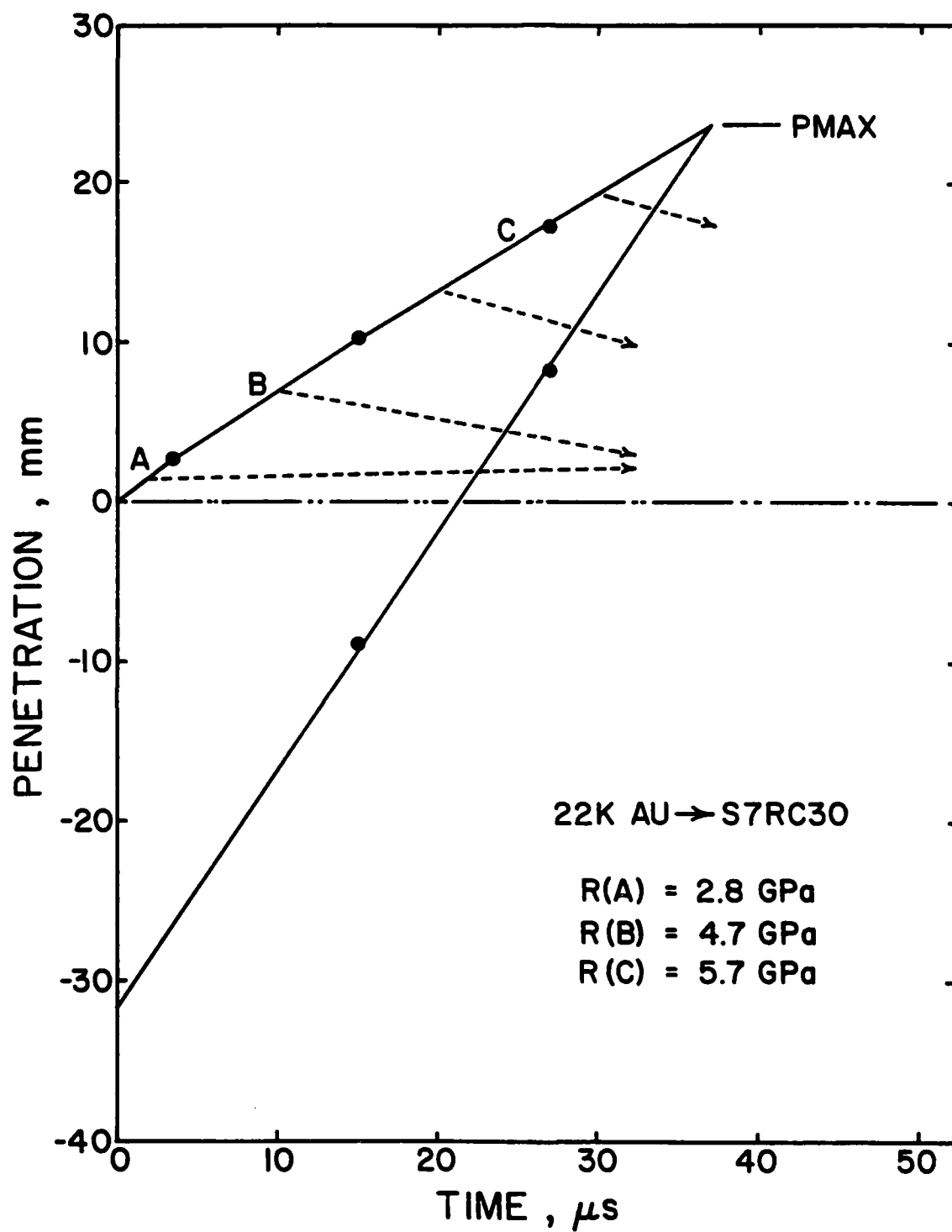


Figure 15. Penetration-Time Plot for a Unitary Gold-Alloy Rod Penetrating Steel.

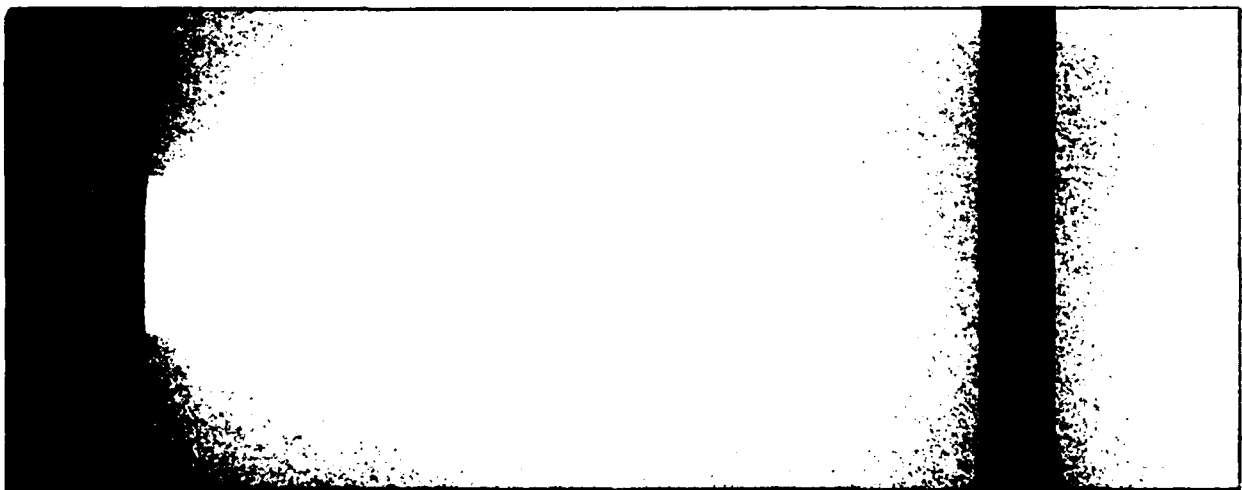
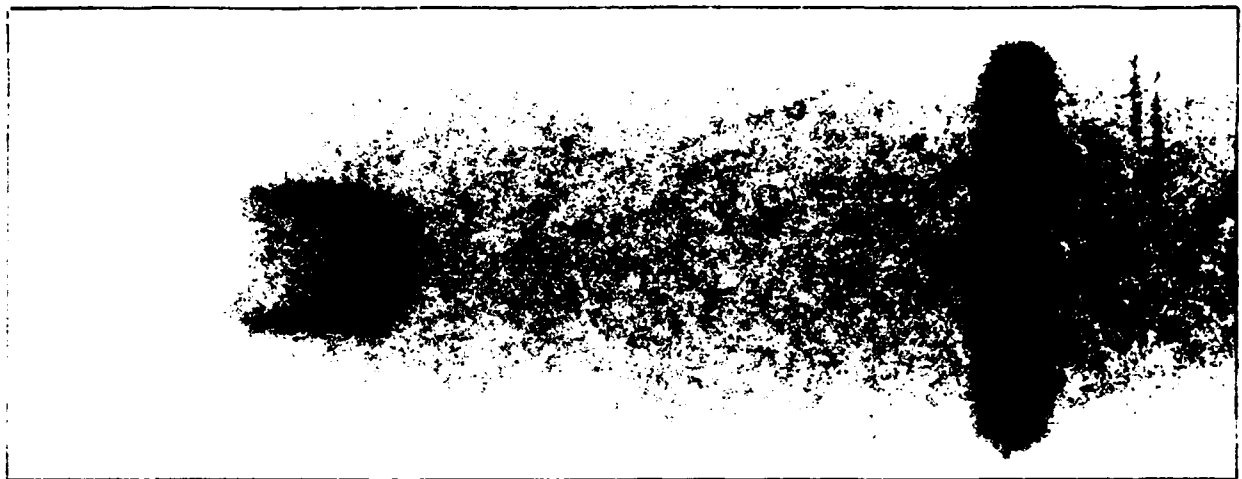


Figure 16. Radiographs Showing Penetration by a Single Gold-Alloy Segment.

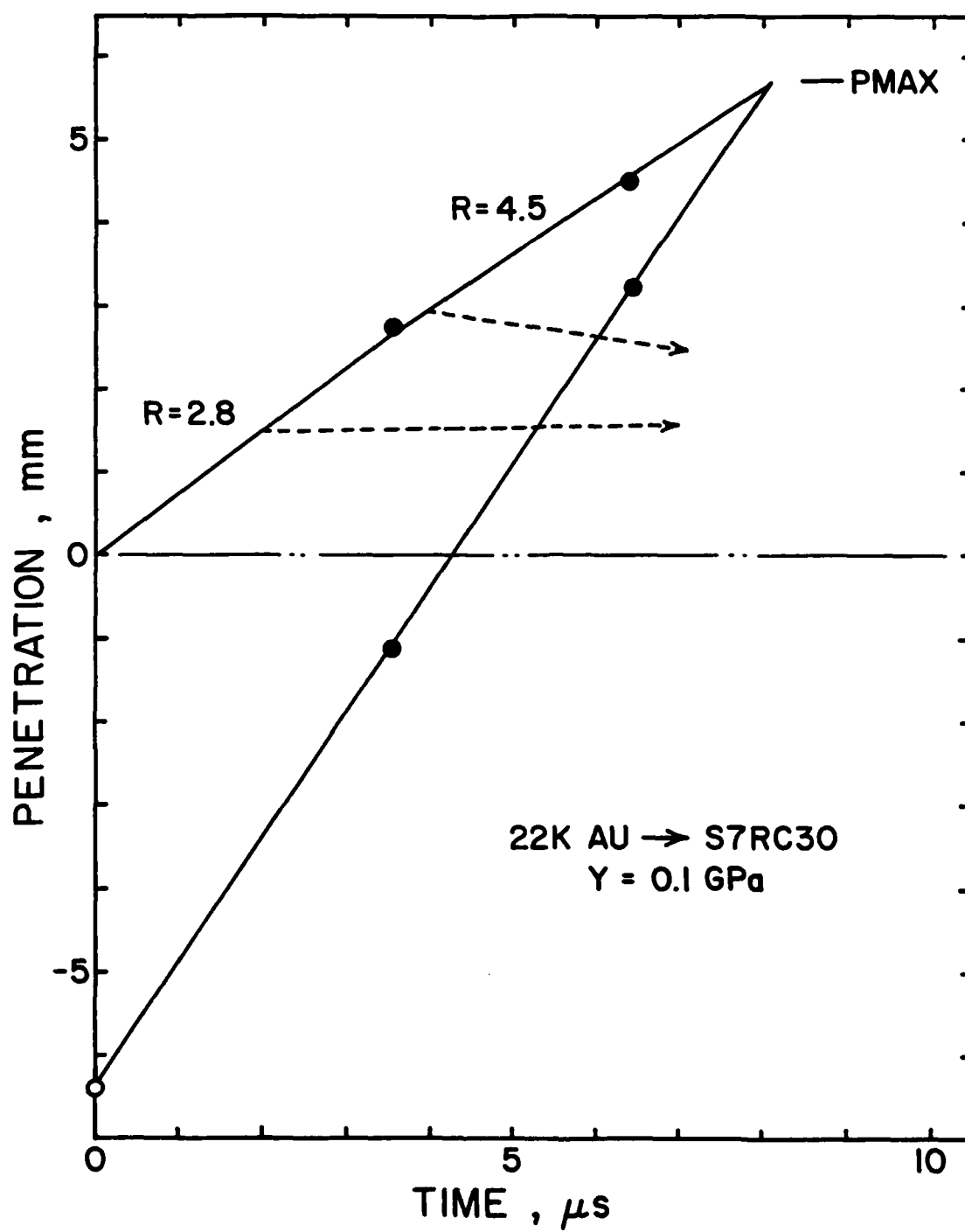


Figure 17. Penetration-Time Plot for a Single Gold-Alloy Segment Penetrating Steel.

3.9 Experiment (AU, 5, 4, 1). Flash radiographs from the experiment with five gold-alloy segments are shown in Figure 18. The upper radiograph shows the third and fourth segments while the lower radiograph shows the fourth and fifth segments. In the upper radiograph, the front portion of the third segment is missing, having apparently been eroded away by an encounter with erosion products from the first two segments. Therefore, the end of the penetration cavity in that radiograph defines the depth of penetration achieved by the first two segments. In the lower radiograph, the fifth segment has suffered significant damage even though it is only a short distance into the penetration cavity. A dense accumulation of erosion products fills the forward portion of the penetration cavity, making it difficult to resolve detail with a high level of confidence.

Data and analysis for this experiment are presented in Figure 19. The analysis was aided by the low strength of the gold alloy which made it possible to rule out changes in velocity and assign all loss of performance to loss of length. The analysis indicated a 22% loss from the second segment, a 76% loss from both the third and fourth segments, and an 84% loss from the fifth segment, with a final penetration depth of only 14.0 mm. There is uncertainty about exact length reductions, and it would be reasonable to expect greater loss from the fourth segment than from the third. However, the high losses are representative of the severe damage suffered during the encounter of low strength segments with erosion products in the penetration cavity.

3.10 Experiments (WA/AL, 5, 4, 1) and (WA/SS, 5, 4, 1). Two experiments and several complementary tests were conducted to examine the possible benefit from supporting segments within thin-wall tubes of aluminum or stainless steel. Aluminum tubes had a wall thickness of 0.38 mm, while the steel tubes had a wall thickness of 0.25 mm. Results could not be interpreted in a penetration-time format, but the influence on final penetration was determined, and some features in the flash radiographs may be worth noting. Before testing segments, one test was conducted with a unitary tungsten-alloy rod ($L/D=20$) in an aluminum tube. The diameter of the penetration path was increased, but the depth of penetration remained unchanged. With five segments and spacing of one segment length, a supporting aluminum tube increased the final penetration to 19.5 mm, an increase of almost 23% over the penetration depth by free-standing segments. With an identical configuration of segments in a steel tube, the depth of penetration was increased to 20.9 mm, an increase of more than 31% over the penetration depth by free-standing segments. The reason for greater penetration by segments supported in a tube cannot presently be attributed to any single factor. The larger diameter of the penetration

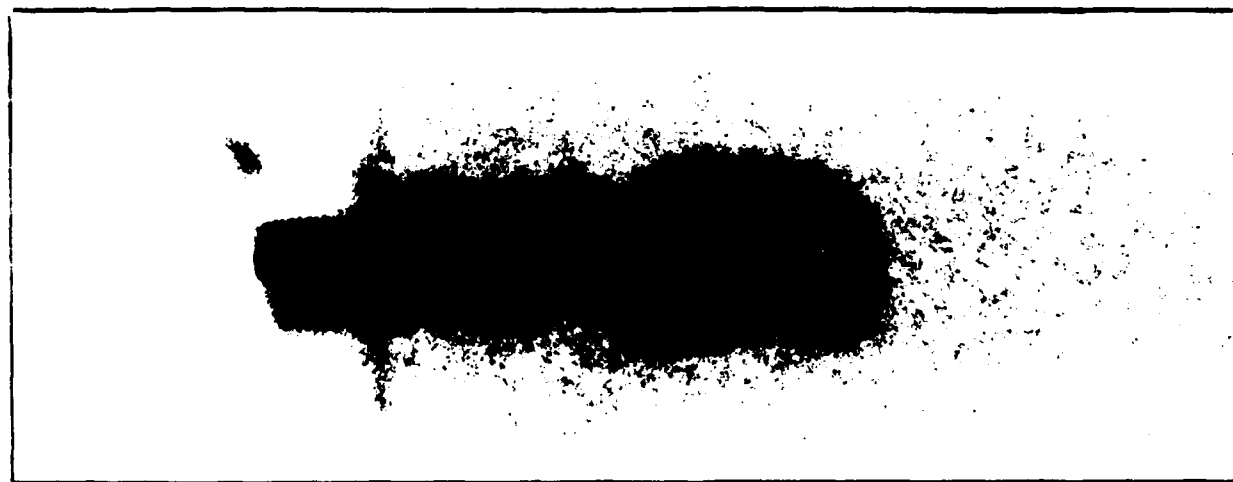
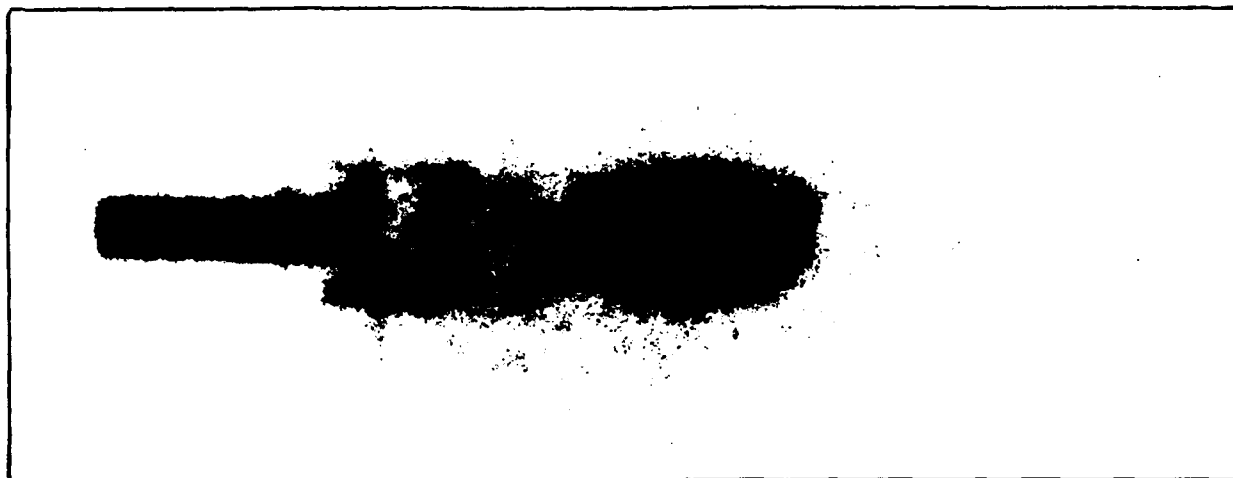


Figure 18. Radiographs Showing Penetration by Five Gold-Alloy Segments.

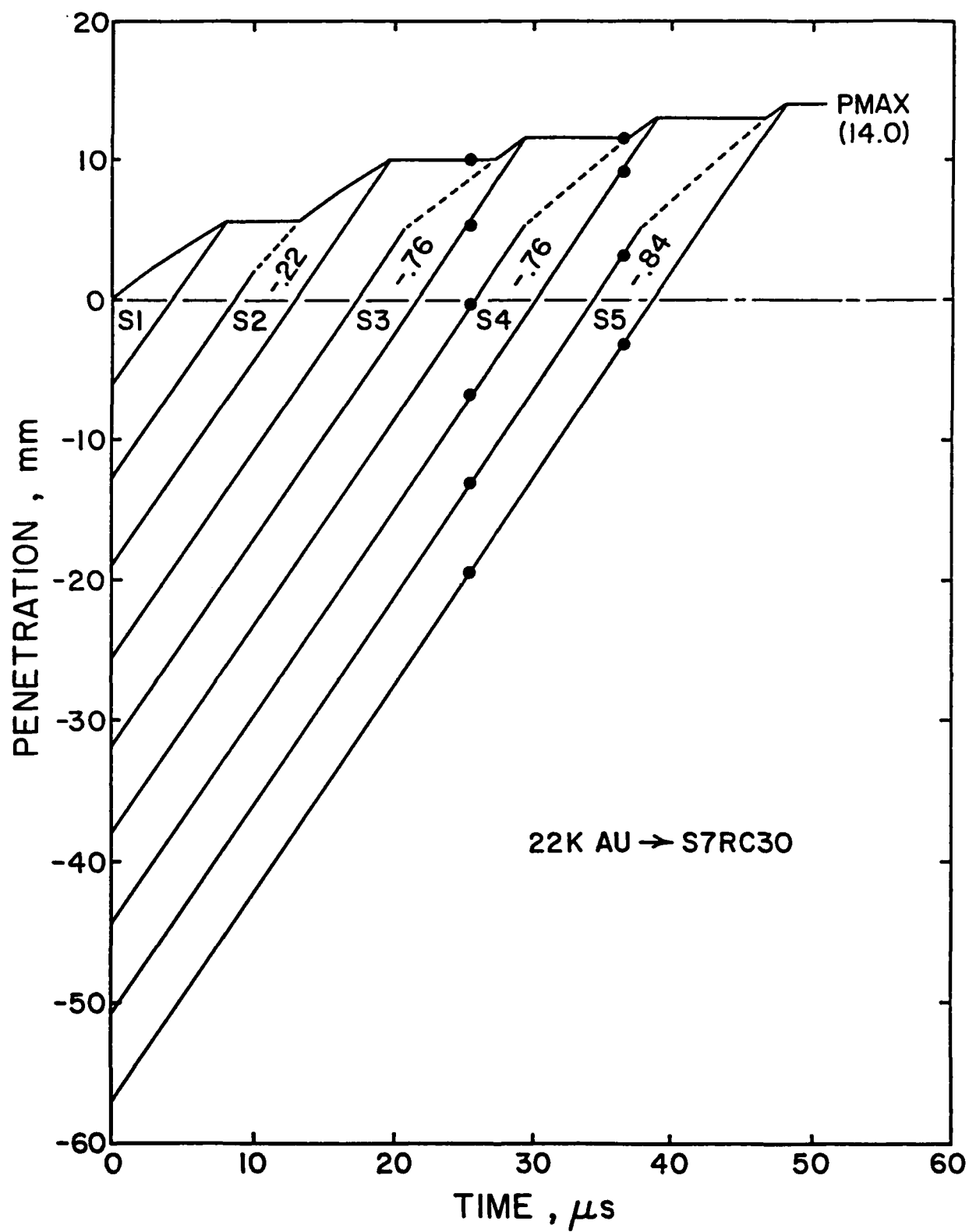


Figure 19. Penetration-Time Plot for Five Gold-Alloy Segments Penetrating Steel.

cavity may tend to reduce the interaction with high-density erosion products. It is also possible that the supporting tube tends to shield the segments from erosion products. Finally, the length of tubing between segments may penetrate and displace part of the tungsten-alloy residue deposited at the end of penetration. For example, the length of steel tubing between segments has the ability to penetrate about 0.73 mm of target steel. The aluminum tubing would not be expected to have much penetrating capability, but it might be marginally effective against the residue, much of which is at an advanced stage of failure.

4. CONCLUSION AND DISCUSSION

The primary conclusion of this study is that the performance of segments was reduced by interactions with residue and erosion products. However, it is important to recognize that tests were conducted at a relatively low velocity where segments should not be most efficient, and that the relatively high L/D ratio does not efficiently utilize the transient high-pressure phase of penetration. At higher impact velocities, deposits of residue would be reduced or eliminated, the penetration cavity should have a larger diameter, and cavity growth by after flow should be enhanced. Also, if segments had a smaller L/D ratio, the scalloped hole profile should be less pronounced and this might reduce the tendency for erosion products to migrate toward the axis of penetration. However, any reduction in residue means an increase in the quantity of erosion products, and at higher impact velocities, high-density erosion products would all travel into a steel target. Although it is possible that these erosion products would not interact with trailing segments to reduce their performance, there is some evidence from shaped charge studies that erosion products can be a factor in the velocity range from 1,500 to 8,000 m/s. In experiments with small shaped charges, Netherwood and Benck (1988) have shown that when erosion products are prevented from escaping at interfaces in a steel target and consequently are confined to the penetration cavity, the penetration by a small copper jet is reduced by nearly 40%. Therefore, even at higher velocities, interactions with erosion products may become a practical concern when a series of high-density segments attack a monobloc steel target.

5. REFERENCES

- Pack, D. C., and W. M. Evans. "Penetration by High-Velocity (Munroe) Jets: I," Proceedings of the Physical Society of London. B64, pp. 298-302, 1951.
- Christman, D. R., and J. W. Gehring. "Analysis of High-Velocity Projectile Penetration Mechanics," Journal of Applied Physics. Vol. 37, pp. 1579-1587, 1966.
- Tate, A. "Long Rod Penetration Models - Part II. Extensions to the Hydrodynamic Theory of Penetration," International Journal of Mechanical Sciences. Vol. 28, pp. 599-612, 1986.
- Aleksevsii, V. P. "Penetration of a Rod into a Target at High Velocity," Combustion, Explosion and Shock Waves. (English Translation), Vol. 2, pp. 99-106, 1966.
- Tate, A. "A Theory for the Deceleration of Long Rods After Impact," Journal of the Mechanics and Physics of Solids. Vol. 15, pp. 387-399, 1967.
- Tate, A. "Further Results in the Theory of Long Rod Penetration," Journal of the Mechanics and Physics of Solids. Vol. 17, pp. 141-150, 1969.
- Wright, T. W. "A Survey of Penetration Mechanics for Long Rods." BRL-TR-02496, U. S. Army Ballistic Research Laboratory, Aberdeen Proving Ground, MD, June 1983.
- Wright, T. W., and K. Frank. "Approaches to Penetration Problems," Proceedings of the First International Conference on Effects of Fast Transient Loadings. Lausanne, pp. 85-103, August 1987.
- Netherwood, P. H., and R. F. Benck. Private communication, U. S. Army Ballistic Research Laboratory, Aberdeen Proving Ground, MD, 24 October 1988.

INTENTIONALLY LEFT BLANK.

<u>No of</u> <u>Copies</u>	<u>Organization</u>
1	Office of the Secretary of Defense OUSD(A) Director, Live Fire Testing ATTN: James F. O'Bryon Washington, DC 20301-3110
2	Administrator Defense Technical Info Center ATTN: DTIC-DDA Cameron Station Alexandria, VA 22304-6145
1	HQDA (SARD-TR) WASH DC 20310-0001
1	Commander US Army Materiel Command ATTN: AMCDRA-ST 5001 Fisenhower Avenue Alexandria, VA 22333-0001
1	Commander US Army Laboratory Command ATTN: AMSLC-DL Adelphi, MD 20783-1145
2	Commander US Army, ARDEC ATTN: SMCAR-IMI-I Picatinny Arsenal, NJ 07806-5000
2	Commander US Army, ARDEC ATTN: SMCAR-TDC Picatinny Arsenal, NJ 07806-5000
1	Director Benet Weapons Laboratory US Army, ARDEC ATTN: SMCAR-CCB-TL Watervliet, NY 12189-4050
1	Commander US Army Armament, Munitions and Chemical Command ATTN: SMCAR-ESP-L Rock Island, IL 61299-5000
1	Commander US Army Aviation Systems Command ATTN: AMSAV-DACL 4300 Goodfellow Blvd. St. Louis, MO 63120-1798

<u>No of</u> <u>Copies</u>	<u>Organization</u>
1	Director US Army Aviation Research and Technology Activity ATTN: SAVRT-R (Library) M/S 219-3 Ames Research Center Moffett Field, CA 94035-1000
1	Commander US Army Missile Command ATTN: AMSMI-RD-CS-R (DOC) Redstone Arsenal, AL 35898-5010
1	Commander US Army Tank-Automotive Command ATTN: AMSTA-TSL (Technical Library) Warren, MI 48397-5000
1	Director US Army TRADOC Analysis Command ATTN: ATAA-SL White Sands Missile Range, NM 88002-5502
(Class. only) 1	Commandant US Army Infantry School ATTN: ATSH-CD (Security Mgr.) Fort Benning, GA 31905-5660
(Unclass. only) 1	Commandant US Army Infantry School ATTN: ATSH-CD-CSO-OR Fort Benning, GA 31905-5660
1	Air Force Armament Laboratory ATTN: AFATL/DLODL Eglin AFB, FL 32542-5000
	<u>Aberdeen Proving Ground</u>
2	Dir, USAMSAA ATTN: AMXSY-D AMXSY-MP, H. Cohen
1	Cdr, USATECOM ATTN: AMSTE-TD
3	Cdr, CRDEC, AMCCOM ATTN: SMCCR-RSP-A SMCCR-MU SMCCR-MSI
1	Dir, VLAMO ATTN: AMSLC-VL-D

<u>No. of Copies</u>	<u>Organization</u>
2	US Army Research Office ATTN: Dr. I. Ahmad Dr. K. Iyer P. O. Box 12211 Research Triangle Park, NC 27709
3	Director US Army Materials Technology Laboratory ATTN: SLCMT-MRD, Dr. G. Bishop Dr. S-C Chou Dr. D. Dandekar Arsenal Street Watertown, MA 02172-0001
2	Director Defense Advanced Research Projects Agency ATTN: Dr. J. Richardson MAJ R. Lundberg 1400 Wilson Blvd. Arlington, VA 22209-2308
2	Lawrence Livermore National Laboratory ATTN: Dr. J. Reaugh, MS L-290 Mr. A. Holt, MS L-321 P. O. Box 808 Livermore, CA 94550
2	Los Alamos National Laboratory ATTN: Mr. B. M. Hogan, MS K574 Dr. G. E. Cort, MS K574 P. O. Box 1663 Los Alamos, NM 87545
2	General Research Corporation ATTN: Dr. A. Charters Dr. T. Menna 5383 Hollister Ave. Santa Barbara, CA 93160-6770
1	Southwest Research Institute ATTN: Dr. C. E. Anderson, Div. 6 P. O. Drawer 28510 San Antonio, TX 78284

<u>No. of Copies</u>	<u>Organization</u>
1	California Research and Technology ATTN: Dr. Dennis Orphal 5117 Johnson Drive Pleasanton, CA 94566
1	Kaman Sciences Corporation ATTN: D. Elder P. O. Box 7463 Colorado Springs, CO 80933
5	LTV Missiles and Electronics Group ATTN: Dr. Gary Hough (WT-50) Mr. K. W. Havens (EM-36) Dr. G. L. Jackson (WT-71) Mr. R. J. Taylor (EM-36) Dr. M. M. Tower (WT-78) P. O. Box 65003 Dallas, TX 75265-0003
1	Zernow Technical Services, Inc. ATTN: Dr. L. Zernow 425 W. Bonita Ave., Suite 208 San Dimas, CA 91773
1	Systems, Science and Software, Inc. ATTN: Dr. R. Sedgwick 3398 Carmel Mountain Road San Diego, CA 92121
1	Battelle - Columbus Laboratories ATTN: R. Jameson 505 King Ave. Columbus, OH 43201

Foreign Distribution

RARDE(FH)
ATTN: Mr. Addison Tat
Sevenoaks
Kent TN14 7BP
United Kingdom

Centre D'Etudes de Gramat
ATTN: Mr. Gerard Solve
46500 Gramat, France

German-French Research Institute (ISL)
ATTN: Mr. Erich Wollman
12 Rue de l'Industrie
68301 Saint Louis, France

Ernst-Mach-Institut
ATTN: Dr. Volker Hohler
Eckerstrasse 4
D - 7800 Freiburg i. Br., FRG

Ernst-Mach-Institut
ATTN: Dr. Alois J. Stulp
Eckerstrasse 4
D - 7800 Freiburg i. Br., FRG

General Dynamics
ATTN: J. H. Cuadros
P. O. Box 50-800
Mail Zone 601-87
Ontario, Canada 91761-6770

INTENTIONALLY LEFT BLANK.

USER EVALUATION SHEET/CHANGE OF ADDRESS

This Laboratory undertakes a continuing effort to improve the quality of the reports it publishes. Your comments/answers to the items/questions below will aid us in our efforts.

1. BRL Report Number BRL-TR-3129 Date of Report JULY 1990
2. Date Report Received _____
3. Does this report satisfy a need? (Comment on purpose, related project, or other area of interest for which the report will be used.) _____

4. Specifically, how is the report being used? (Information source, design data, procedure, source of ideas, etc.) _____

5. Has the information in this report led to any quantitative savings as far as man-hours or dollars saved, operating costs avoided, or efficiencies achieved, etc? If so, please elaborate. _____

6. General Comments. What do you think should be changed to improve future reports? (Indicate changes to organization, technical content, format, etc.) _____

CURRENT ADDRESS

Name

Organization

Address

City, State, Zip Code

7. If indicating a Change of Address or Address Correction, please provide the New or Correct Address in Block 6 above and the Old or Incorrect address below.

OLD ADDRESS

Name

Organization

Address

City, State, Zip Code

(Remove this sheet, fold as indicated, staple or tape closed, and mail.)

-----FOLD HERE-----

DEPARTMENT OF THE ARMY

Director
U.S. Army Ballistic Research Laboratory
ATTN: SLCBR-DD-T
Aberdeen Proving Ground, MD 21005-5066
OFFICIAL BUSINESS



NO POSTAGE
NECESSARY
IF MAILED
IN THE
UNITED STATES

BUSINESS REPLY MAIL
FIRST CLASS PERMIT No 0001, APG, MD

POSTAGE WILL BE PAID BY ADDRESSEE

Director
U.S. Army Ballistic Research Laboratory
ATTN: SLCBR-DD-T
Aberdeen Proving Ground, MD 21005-9989

-----FOLD HERE-----